MEASUREMENT OF NEUTRON SPECTRA AND FLUXES AT THE IPNS RADIATION EFFECTS FACILITY

R. C. Birtcher, M. A. Kirk, T. H. Blewitt and L. R. Greenwood

Argonne National Laboratory
Argonne, Illinois 60439

ABSTRACT

We have measured the neutron spectra, fluxes, and flux distributions produced by nuclear spallation resulting from 478-MeV proton bombardment of tantalum and depleted uranium targets surrounded by a thick lead neutron reflector. The configuration was chosen to simulate a radiation effects facility at a spallation-neutron source. The method of multiple foil activation with spectrum unfolding by the STAYSL computer code was used to measure the neutron spectra. The experimental results are compared in detail with the results of computer calculations on the same configuration of targets and reflector. The neutron production and transport codes HETC and VIM were employed in these calculations.

Based on these measurements, the Radiation Effects Facility (REF) was designed and constructed at the IPNS. Using simular activation techniques the neutron spectra, fluxes and flux distributions have been determined for the REF.

1. INTRODUCTION

The Development of nuclear reactors as energy sources has required and will continue to require the study of the effects of neutron irradiations upon materials. This has lead to the need for a Radiation Effects Facility (REF) at the IPNS [1].The study of radiation effects requires well-controlled intense fluxes of high-energy neutrons without contamination by secondary particles. Further, access to these neutrons must be direct and allow precise environment and temperature control. Many basic studies also require

irradiation at liquid helium temperatures to arrest defect migration. These requirements have placed several restrictions upon the design of the REF. The proton target should generate the largest number of neutrons per proton with the minimum of neutron-energy moderation and minimum γ flux. This led to the minimization of the target cooling water and target diameter consistant with acceptable target temperatures. Both Ta and ^{238}U were considered as target materials. To further minimize the neutron energy loss and increase the neutron flux, the target should be surrounded by a high density reflector material consisting of atoms with a high atomic number. These considerations lead to the testing of several target/reflector systems by computer modeling and finally by a full scale experimental mock-up [2].

2. Experimental Details

2.1 Mock-up.

A simplified schematic of the experimental arrangement for the REF mock-up is shown in Fig. 1. The targets were solid cylinders of Ta, 8.2 cm in diameter and 13.2 cm long, and of Zircaloy-clad ^{238}U, 8.3 cm in diameter and 14.6 cm long. Each target was irradiated separately while centrally located in a cylindrical Pb cask. The Pb cask surrounded the target with 25 cm of reflector material, and held the neutron-dosimetry assemblies. The perpendicular neutron dosimetry assembly was located in a hole that passed within 1 cm of the ID surface of the cask. The target was located so that this hole was at the calculated peak neutron flux position along the target axis. The principal neutron dosimetry package was also located within the hole, and adjacent to the target. The parallel neutron dosimetry assembly was located in an Al tube suspended between the Pb cask and the target. An additional 46 cm of Pb was placed above and on one side of the Pb cask for radiation shielding of the environment. The entire target and cask were electrically isolated to provide a Faraday-cup measurement of incident-proton current. This and another Faraday-cup beam stop were used to monitor beam alignment on target during the irradiation, but proved to be substantially in error for an absolute measurement of integrated proton current over the entire irradiation period. Instead, the integrated proton flux was measured with Al monitor foils, as described in the next subsection.

Both targets were water cooled with a flow of ~0.6 l/sec. Temperatures were monitored by thermocouples during irradiations by 478-MeV protons at

typical time-averaged currents of ~1 μA. The temperature increased by ~2°C

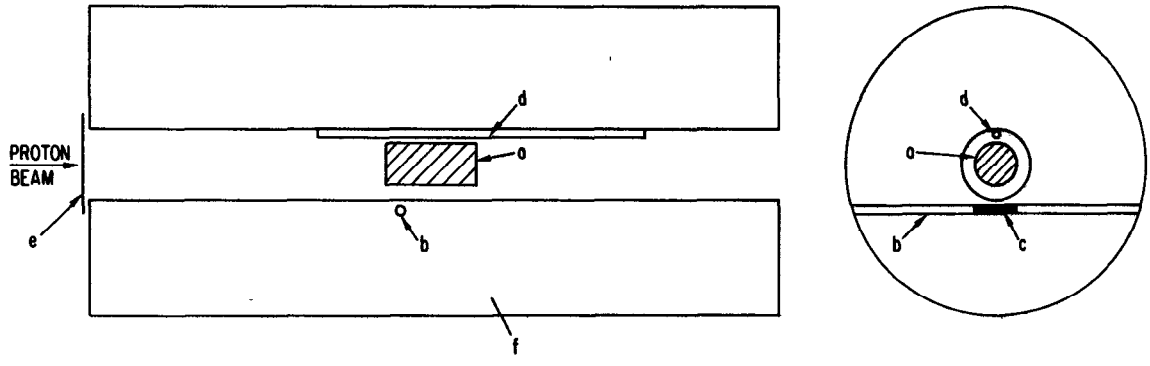

Figure 1. Schematic of target, reflector, and dosimetry positions. (a) Ta or ^{288}U target; (b) hole for perpendicular neutron dosimetry assembly; (c) principal neutron dosimetry site; (d) tube for parallel neutron dosimetry assembly; (e) proton dosimetry foils; and (f) Pd reflector.

above the coolant temperature (35°C) on the surface of the Ta target at the calculated axial position of maximum energy deposition (5 cm from the front face of the target). There was a ~35°C rise in the centerline temperature at a similar axial position in the ^{238}U target.

The 478-MeV proton beam was supplied to the mock-up experiment by the ANL Rapid Cycling Synchrotron (RCS, formerly called Booster II [3] when associated with the ZGS accelerator). The protons were obtained by stripping the electrons from a 50-MeV H^- beam supplied by a linear accelerator (Linac), which also served to inject the ZGS during these experiments. As a result of the sharing of the Linac system with the ZGS, the RCS was operated in a "burst mode", consisting of approximately 2.7 seconds of beam extraction at 15-Hz repetition, followed by 1.3 seconds without beam. This mode of operation had no effect on the operation of the experiment or the results. The number of protons per pulse on target averaged ~7 x 10^{11} with an effective frequency of ~10 Hz as a result of the burst-mode operation, yielding an average beam current on target of about 1 μA during normal operation of the accelerator. "Abnormal" accelerator operation consisted of complete shutdowns due to equipment failures. Details of the accelerator operation were recorded for each irradiation, and used to correct the corresponding neutron dosimetry data.

Integral dosimetry of the 478-MeV proton beam was accomplished by monitoring the ^{27}Al (p,x) ^{22}Na reaction in aluminum foils placed at the entrance to the Pb reflector (Fig. 1). A cross section of 17.8 mb (±15%) was

used for the ^{27}Al (p,x) ^{22}Na reaction at the proton energy of 478 MeV. This cross section is the value recommended by the CEA (France) in their 1971 compilation of nuclear monitor reactions [4]. The error represents the spread of the various experimental data at this energy. The uncertainty in the value of this cross section is the predominant source of possible error in the absolute number of protons on target. To compensate for the loss of energetic spallation products at the surfaces of the Al foil, a high-purity Al foil 0.025 mm thick was sandwiched between two ordinary Al foils 0.012 mm thick. These foil thicknesses proved adequate to compensate for loss of the ^{22}Na product, but inadequate for the lighter ^{7}Be product. For this reason, and because the cross section for its production is not as well established, the ^{7}Be activity was not used for dosimetry purposes. The proton spallation reaction yielding ^{24}Na was not used for proton dosimetry because ^{24}Na is produced by neutron absorption in Al and because of the short ^{24}Na half-life (15 hr).

The Al dosimetry foils were also used to obtain autoradiographs of the integrated intensity distribution of the proton beam for each target irradiation. Microphotodensitometry data were obtained from the autoradiographs to generate the experimental beam profiles (linearity with fluence was assumed), which were then averaged about the cylindrical axes of the targets. These averaged radial beam profiles were used as input parameters to the computer programs that calculated the spallation-neutron production with which the experimental results will be compared. The proton beam for irradiation of the ^{238}U target was intentionally broadened somewhat to lower the target centerline temperature.

2.2 Computer Model Calculations.

Spallation-neutron production and neutron transport were calculated by two Monte Carlo-based three-dimensional computer codes, HETC [5] and VIM [6]. The High Energy Transport Code (HETC) employs nuclear models to calculate high-energy-cascade and evaporation particles caused by the incident protons. Spallation neutrons with energies from 500 MeV down to 15 MeV were transported by this code to the volumes in which the experimental measurements were made. Neutrons with $E_n < 15$ MeV were subsequently transported by the VIM code. Neutron-produced fission in the ^{238}U target was included in the VIM

calculations, but not in the NETC calculations.

The detailed geometry and material composition of the target, cooling system, and reflector were taken into account in the calculations of the mock-up experiment. Neutron spectra, integrated flux, and spatial flux distributions were obtained for each target by averaging three independent calculations, each involving 2000 incident 500 MeV protons distributed on the target face according to the experimental beam profile. The results of these calculations will be displayed and compared with the experimental dosimetry results in section.

2.3 Radiation Effects Facility

The REF, shown in Fig. 2, consists of the ^{238}U target, two vertical irradiation thimbles, and a horizontal irradiation thimble, all surrounded by a Pb neutron reflector. Based on the results of the mock-up experiment, the target material was chosen to maximize the conversion of protons to neutrons. There is some gamma production associated with the fission process in ^{238}U, although much less than in a reactor-based facility where all neutrons are produced by fission. Should the gamma flux pose an experimental problem, it is possible to change to a Ta target, from which there would be a greatly reduced gamma flux. Lead was chosen as the reflector material based on the results of the mock-up experiment. The Pb reflector alongside the target is in the form of removable sections 10 cm on a side and 45 cm long in cladding. For specialized needs, reflector sections can be removed to increase the irradiation volume or to allow replacement with a different reflector material. Such a change in reflector or target material could change the energy distribution of the neutrons within the irradiation facilities.

The two vertical irradiation thimbles, located on either side of the target at the positions of maximum flux, contain liquid helium cryostats (5 cm inner diameter) that can operate at temperatures between 4 and 1000 K. The liquid helium is supplied by a single 400-W refrigerator (CTI model 2800 R). The two cryostats have separate vacuum systems, which allow the temperature to be controlled independently in each cryostat. The horizontal irradiation thimble (2 cm inner diameter) is located on an axis parallel to and directly below the target. The majority of the ^{238}U target-cooling water is between

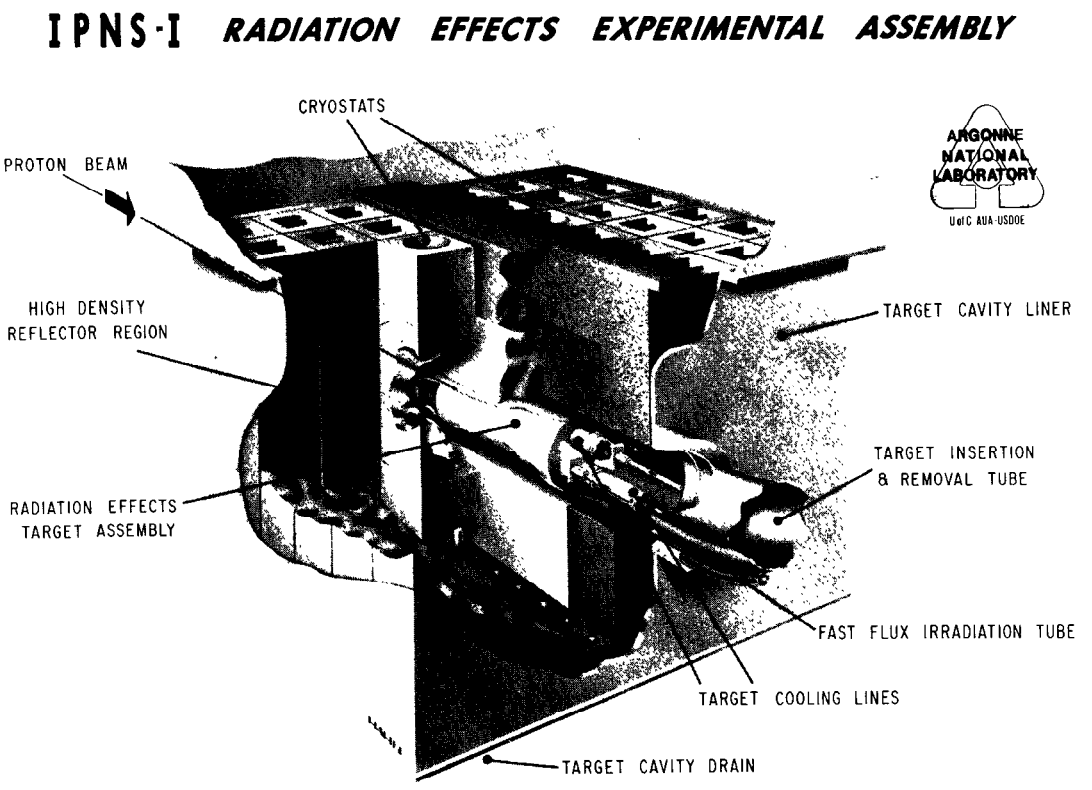

Figure 2. IPNS-I radiation effects assembly.

the target and this thimble. The horizontal thimble operates at ambient temperature and is designed to permit short irradiations with sample removal while neutrons are being produced. The REF differs from the mock-up experiment in the large voids near the target.

2.4 Neutron Scattering Facility

The ^{238}U target in the NSF is surrounded by C and Be reflectors which are penetrated by 12 neutron beam lines. Moderators for producing the thermal-neutron beams are located directly above and below the target. Two unused horizontal beam lines have been modified to contain irradiation thimbles (~1 cm diameter). These two thimbles radially approach within 4 cm of the target axis at the position of maximum neutron flux along this. The majority of target-cooling water is between the target and these thimbles. Both NSF irradiation thimbles operate a ambient temperature.

Protons for the IPNS were supplied by the RCS at 500 MeV [7]. The protons were ~100 ns long pulses at a repetition rate of 30 Hz. The proton flux incident upon the ^{238}U targets was determined from the current induced in

a toroid located 3.5 m upstream from the target. This measurement is uncertain by 5 percent. The protons had an energy of 500 MeV.

2.5 Neutron Dosimetry.

A multiple-foil-activation method was used to determine the neutron fluxes and energy spectra for the Ta and ^{238}U irradiations at the principal dosimetry site in the mock-up experiment (Fig. 1) and at the primary irradiation positions in the irradiation facilities. The STAYSL computer code [8] was used to find the most probable neutron spectra from the foil acitivies, using a least-squares technique. The input spectra were taken from the computer-model calculations of neutron production and transport to the principal dosimetry site for each target and reflector system.

The Dosimetry Group and the Analytical Chemistry Laboratory at ANL measured foil activities with Ge(Li) detectors over several γ-decay half-lives for each of the 28 reactions listed in Table 1. Peak integrations and Compton-background subtractions were done by means of computer programs in routine use by the Dosimetry Group [9]. Prior to spectrum unfolding, activation corrections for neutron and gamma self-shielding, cover foils, and decay during and after irradiation were made for foil geometries in an isotropic flux. The STAYSL program compared the calculated activities with the measured activities. It then adjusted the differential neutron spectrum (100 energy groups), using a least-squares procedure. The energy-dependent cross sections were taken from ENDF/B-IV [10]. For those reactions sensitive to neutron energies $\gtrsim$ 30 MeV, the energy-dependent cross sections have been extrapolated [11] to 44 MeV and integrally tested in a well-defined Be (d,n) neutron spectra [12].

The output of the STAYSL code includes a complete covariance-error matrix for the neutron-flux spectra. Errors and covariances in the measured acitivities, cross sections, and input spectra were estimated from the available nuclear data. The integral activities typically had errors of ±2%, whereas cross-section and flux errors varied from 5 to 50% depending on the estimated reliability of nuclear data. Flux and cross-section self-covariances were specified by a Gaussian function assuming that nearby groups are highly correlated and widely separated groups uncorrelated. This procedure also guarantees a smooth output spectra, avoiding sharp peaks and

Table 1. Neutron dosimetry reactions

Material	Reaction	Half-life (days)	Cd Cover[a]
^{235}U	$(n,f)^{95}Zr$, ^{103}Ru, ^{140}Ba	64.1,39.4,12.8	+[a]
^{237}Np	$(n,f)^{95}Zr$, ^{103}Ru, ^{140}Ba[b]	64.1,39.4,12.8	+
	$(n,\gamma)^{238}Np$[b]	2.1	+
^{238}U	$(n,f)^{95}Zr$, ^{103}Ru, ^{140}Ba	64.1,39.4,12.8	-
	$(n,\gamma)^{239}Np$	2.36	+
	$(n,2n)^{237}U$	6.75	-
Ni	$^{58}Ni(n,p)^{58}Co$	70.85	-
	$(n,2n)^{57}Ni$	1.5	-
Fe	$^{54}Fe(n,p)^{54}Mn$[b]	312.5	-
	$(n,\alpha)^{51}Cr$[b]	27.7	-
	$^{58}Fe(n,\gamma)^{59}Fe$	44.60	+[b]
Au	$^{197}Au(n,\gamma)^{198}Au$[c]	2.7	+
	$(n,2n)^{196}Au$	6.1	-
	$(n,3n)^{195}Au$	184	-
Co	$^{59}Co(n,\gamma)^{60}Co$	1925	+
	$(n,p)^{59}Fe$	44.6	-
	$(n,2n)^{58}Co$	70.85	-
	$(n,3n)^{57}Co$	271	-
	$(n,4n)^{56}Co$[b]	78.5	-
Ti	$^{46}Ti(n,p)^{46}Sc$[b]	88.9	-
	$^{47}Ti(n,p)^{47}Sc$[b]	3.4	-
	$^{48}Ti(n,p)^{48}Sc$	1.8	-
Sc	$^{45}Sc(n,\gamma)^{46}Sc$	88.9	+
	$(n,2n)^{44m}Sc$	2.44	-
Al	$^{27}Al(n,\alpha)^{24}Na$	0.63	-
Nb	$^{93}Nb(n,2n)^{92m}Nb$	10.1	-

[a]"+" means both covered and uncovered samples were included.

[b]Not used for spectral analysis — cross section uncertain.

[c]Both thick and dilute alloy foils.

Proton dosimetry reactions

Material	Reaction	Half-life (days)
Cu	$^{65}Cu(p,n)^{65}Zn$	244
V	$^{51}V(p,n)^{51}Cr$	27.7
LiF	$^{7}Li(p,n)^{7}Re$	53.3

dips at known neutron resonances. The output covariance-error matrix was used to compute broad group flux errors (Table 2) and can be used for errors in derived quantities such as nuclear displacements or gas production in irradiated materials.

In addition, the spatial flux distribution was determined for the two other neutron-dosimetry locations of the mock-up shown in Fig. 1 and in the vertical thimble of the REF, using 50-cm-long dosimetry wires of Fe, Ni, Ti, and Co. After irradiation, the wires were cut into 2.5-cm segments. The neutron spectrum in each segment was calculated by means of STAYSL to fit the activities produced by eight reactions in the wires; the spectrum measured at the corresponding principal disometry site was used as an input spectrum, Integral fluxes ($E > 1.0$ MeV) of the resultant spectra were determined along the length of these two dosimetry locations, but with less accuracy than at the principal site, since fewer neutron reactions were available.

Secondary-proton dosimetry was also performed in a position near the principal neutron dosimetry site. The proton reactions listed in Table 1 for Cu, V, and LiF were used to obtain an approximate estimate of secondary-protron flux and crude energy distribution.

3. Neutron Spectra and Fluxes

3.1 Mock-up

The neutron spectra obtained at the principal dosimetry site of the mock-up experiment are shown in Figs. 3 and 4 for the Ta and ^{238}U targets, respectively. In these two figures, the solid lines are the theoretical calculations (HETC and VIM) and the dotted lines are the results of fitting the experimental foil activities of Table 1 with the STAYSL code, using the calculated spectra as input. In Figs. 3 and 4, the experimental determinations extend to 44 MeV, and the calculated spectra are not displayed above this energy.

For both targets, the agreement between calculated and experimental neutron spectra, is seen to be reasonably good. However, the experimental data tend to yield more neutrons in the energy range between about 10^{-2} and 10^{-1} MeV, and fewer neutrons below 10^{-3} MeV, than one finds in the calculated spectra for the two targets. The remaining differences above 10^{-1} MeV are close to, or within, the experimental error. The experimental error is least

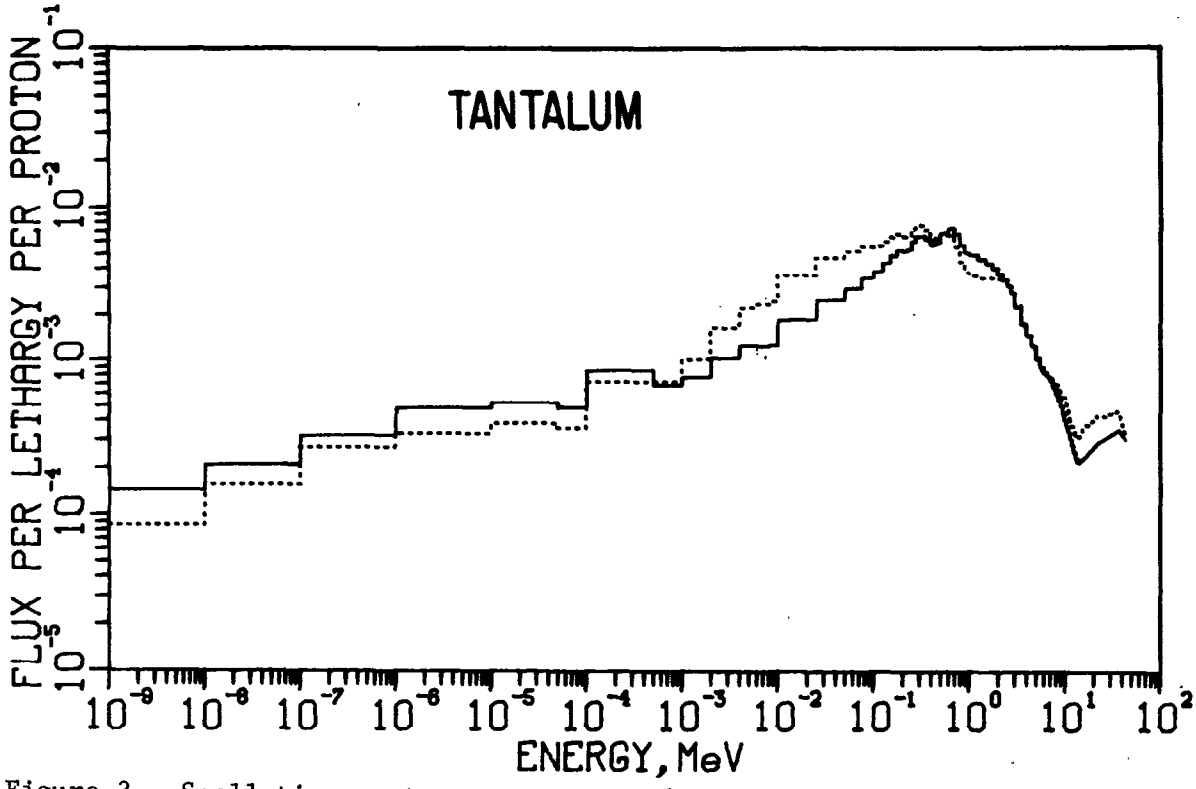

Figure 3. Spallation neutron spectra produced in the mock-up experiment by irradiation of the tantalum target.. The solid line is calculated and the dotted line is experimental.

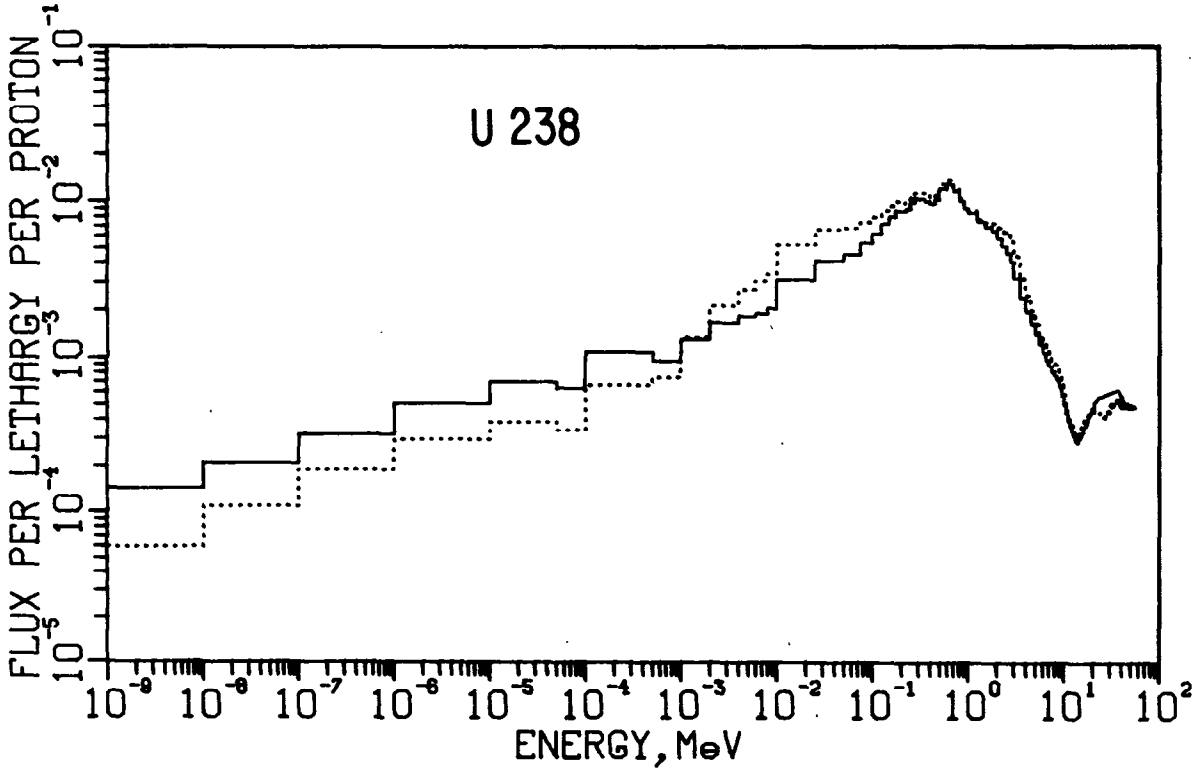

Figure 4. Spallation neutron spectra produced in the mock-up experiment by irradiation of the depleted uranium target. The solid line is calculated and the dotted line is experimental.

where the number of nuclear reactions and the magnitude of the cross sections used in this study are greatest, namely, for neutron energies less than 10^{-3} MeV and between 2 and 10 MeV. However, owing to the strong covariance effects between different neutron-energy groups, reducing the error in energy regions that are well covered by reactions helps to establish the neutron spectrum in the difficult region between 10^{-2} and 2 MeV, and integral errors in fluxes or derived quantities are less than might be expected.

Above 10 MeV, an unexpected bump appears in both calculated and experimental spectra for both target materials. The sharpness of these bumps is due to the method of plotting the flux per unit lethargy ($d\phi/d\ln E$, or equivalently, $E\, d\phi/dE$), which tends to accentuate high-energy features. In a linear differential plot, $d\phi/dE$, this feature becomes a marked change in slope and is also revealed in the calculations of Fullwood et al. [13] In the calculated spectra, this change of slope in the differential plot is the beginning of the high-energy tail of spallation neutrons with energies up to the incident proton energy, or 478 MeV in the present experiment.

The calculated neutron flux falls rapidly above 30 MeV. The neutron flux in the 44-500 MeV energy region was ignored in the spectral measurements, since adequate activation cross sections are not available. However, this omission does not have any significant effect on the output flux solutions, since the flux is falling rapidly with energy and the flux above 44 MeV is less than 1% of the total. In particular, the rise in the lethargy spectra above 14 MeV is not caused by omitting neutrons above 44 MeV, since the reactions which have large cross sections between 10 and 30 MeV have negligible cross sections above 44 MeV. Only the $^{59}Co(n,3n)$ reaction would be significantly affected, probably lowering the flux in the last few energy groups (> 40 MeV) where the uncertainty is already very large.

Only the spectrum for neutron energies > 0.1 MeV is of importance to most radiation-damage phenomena; however, the entire spectrum and neutron yield is of concern for slow neutron scattering studies. Some values of integral flux determined at the principal dosimetry site are displayed in Table 2 for both target systems. The integral flux values for neutrons in several energy ranges are shown, along with the one-standard-deviation error, and are compared with the calculated results for neutron energies > 0.1 MeV and > 1.0 MeV. As a best estimate and for completeness, the calculated flux for neutron

Table 2. Integral neutron fluxes per incident 500 MeV proton

Neutron Energy (MeV)	Neutrons (n/m^2 per proton)						
	Mock-up Ta Target		Mock-up ^{238}U Target		REF Vertical thimble (Center)	REF horizontal thimble	NSF horizontal thimble
	Exp.	Calc.	Exp.	Calc.			
Total	383(±15%)		579(±13%)		311	203	194
Thermal	8.31(±16%)		4.51(±16%)		2.4	1.7	44
> 0.1	209(±21%)	200	362(±17%)	310	199	122	55
> 1.0	60.1(±11%)	63	114(±13%)	93	66	36	13
Secondary Proton Energy (MeV)	Secondary Protons (P/m^2 per proton)						
20-40	~0.3		~0.3		~0.7	~0.2	~0.2

energies > 44 MeV has been added to the experimental determinations of integral fluxes for all lower energy limits. The consequences of this assumption, or any other reasonable assumption for the flux above 44 MeV, are quite small for the total, thermal E_n > 0.1 MeV, and E_n > 1 MeV integral fluxes. The standard-deviation errors for the integral fluxes reflect the uncertainties in the neutron-spectrum determinations. They do not, however, include an overall 15% uncertainty due to possible error in the ^{27}Al (p,x) ^{22}Na cross section (17.8 mb) used to ^{238}U targets, but not to the realtive error between the Ta and ^{238}U results.

It should be noted that the agreement between experimental and calculated values of integrated flux for neutrons with energies > 0.1 MeV is somewhat fortuitous for Ta. With reference to Fig. 3, it can be seen that the integrals of the calculated and experimental curves are equal only if the lower-energy limit is about 0.1 MeV. Other lower-energy limits of integration will result in significant differences between calculated and experimental integrated fluxes.

Also displayed in Table 2 are the results of an attempt to measure the secondary-proton flux present at the principal neutron dosimetry site. The spallation reaction ^{27}Al (p,x) ^{22}Na is of only limited use, owing to probably interference by a similar neutron spallation reaction, ^{27}Al (n,x) ^{22}Na, of unknown cross section. This interference will only take place at the neutron-dosimetry sites that are near the target. The primary-proton dosimetry foils at the front of the Pb reflector (Fig. 1) will not be exposed to a comparable flux of very high-energy neutrons ($\phi_n << \phi_p$). The results of the reactions listed in Table 2 indicate a secondary-proton flux of roughly 0.3 p/m^2 per incident 478-MeV proton, with energy values in the range of 20-40 MeV. The ^{22}Na production can be accounted for by assuming the calculated neutron flux for E_n > 40 MeV and a high-energy neutron cross section for ^{22}Na production equal to the cross section for high-energy protons. The estimate of the secondary-proton flux could be improved considerably through knowledge of the spallation cross section for high-energy neutrons in aluminum. The secondary-proton flux is assumed to be predominantly above 20 MeV, since the cross sections for the proton reactions with Cu, V, and Li all rise steeply below 20 MeV. We would thus expect to observe much greater activation if there were a significant proton flux below 20 MeV. Furthermore, all three activation rates

can be simultaneously fit, assuming most protons are in the 20-40 MeV energy region. In any case, this weak secondary-proton flux does not appear to be significant in terms of either radiation damage in materials or interference with the neutron dosimetry [e.g., the (p,d) reaction is indistinguishable from (n,2n), etc.].

3.2 Radiation Effects Facility

The energy distribution of the neutrons at the position of maximum flux along the center of the REF vertical thimble is shown in Fig. 5 along with the energy distribution for fission neutrons. The neutron flux measurements were made with 1 atm of He gas in the irradiation thimble, and only minor changes are expected if the cryostats contain liquid helium. The REF neutron spectrum can be characterized as a degraded fission spectrum with a high-energy component. The flux of neutrons with $E > 0.1$ MeV is 199 $(n/m^2)/p$, and the ratio of thermal to "fast" ($E > 0.1$ MeV) neutrons is 0.012 for 500-MeV protons incident upon the ^{238}U target. The secondary proton flux is estimated to be 0.7 ± 0.5 $(p/m^2)/p$ or 0.4% of the flux of neutrons with $E > 0.1$ MeV. Radiation of LiF thermal luminescence dosimeters has placed an upper limit on the γ flux of 15% of the total dose in Rads.

The neutron energy distribution for the REF horizontal thimble is also shown in Fig. 5. This spectrum is very similar to the spectrum for the vertical thimble, and the minor differences are likely due to the increased target-cooling water near the horizontal thimble. In the horizontal thimble the flux of neutrons with $E > 0.1$ MeV is 122 $(n/m^2)p$, and the ratio of thermal to "fast" ($E > 0.1$ MeV) neutrons is 0.014 for 400-MeV protons incident upon the ^{238}U target. The lower number of neutrons per proton for the horizontal thimble is due in part to the differences in the distance from the target axis to the horizontal thimble and the vertical irradiation thimbles. The proton flux in the horizontal thimble is estimated to be 0.20 ± 0.15 $(p/m^2)/p$ or 0.2% of the flux of neutrons with $E > 0.1$ MeV. The neutron and proton fluxes at the principle dosimetry sites in the REF are listed in Table 2.

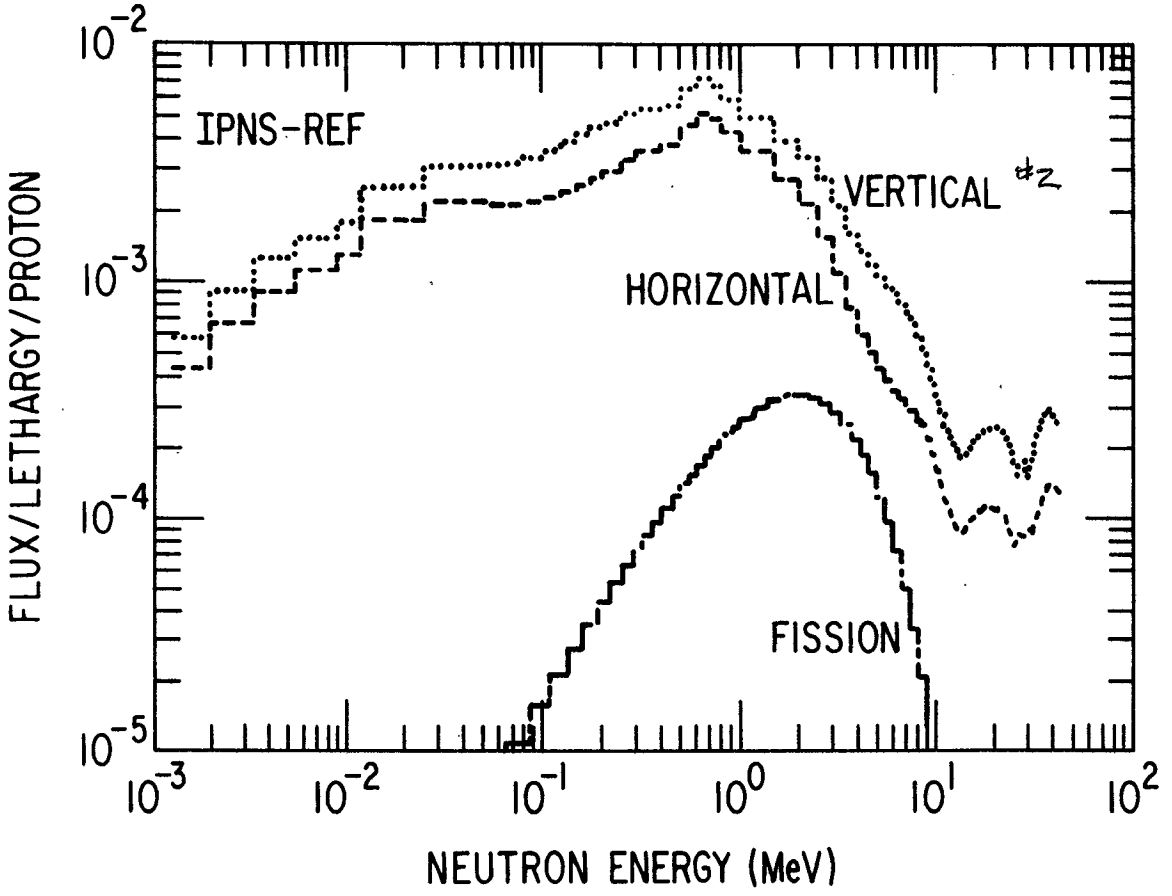

Figure 5. Neutron spectra produced in the vertical and horizontal thimbles of the REF by 500-MeV protons incident upon the ^{238}U target; a pure fission neutron spectrum is shown for comparison.

3.3 Neutron Scattering Facility

Figure 6 shows the neutron energy spectrum for one of the horizontal thimbles in the NSF, the REF vertical thimble, and a pure fission spectrum. The neutron energy distribution for the NSF and REF are quite different, particularly at low neutron energies. The additional low-energy neutrons are produced by (n,2n) reactions and down-scattering in the C and Be. The flux of neutrons with E > 0.1 MeV is 55 $(n/m^2)/p$, and the ratio of thermal to "fast" (E > 0.1 MeV) neutrons is 0.80 for 500-MeV protons incident upon the ^{238}U target. The neutron fluxes available in the NSF are listed in Table 2.

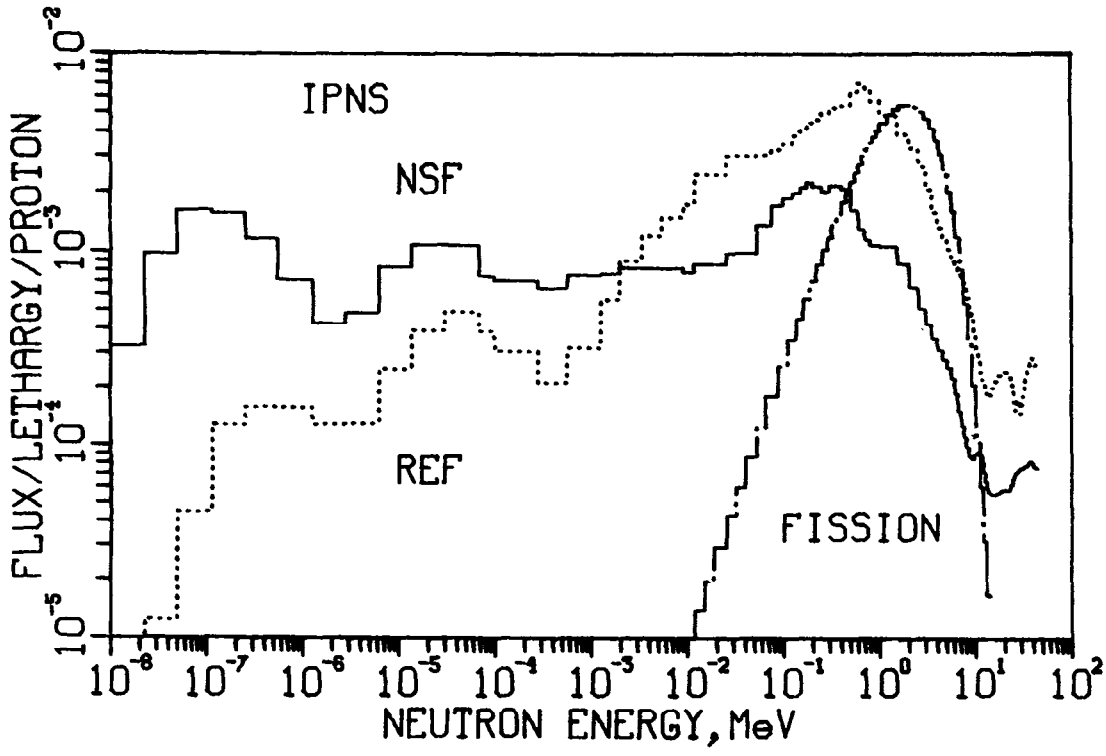

Figure 6. Neutron spectra produced in the REF vertical thimble and NSF horizontal thimble by 500-MeV protons incident upon the ^{238}U targets; a pure fission spectrum is shown for comparison.

4. Spatial Distribution of Neutron Flux

4.1 Mock-up.

All of the above results have been obtained from the complete set of reactions listed in Table 1, determined at the principal dosimetry sites; however, additional data were obtained at the other neutron dosimetry locations shown in Fig. 1, using only eight reactions. Integrated-spatial flux distributions were obtained in directions perpendicular and parallel to the target cylinder axis, though not to the same degree of accuracy as was possible at the principal dosimetry site. Figure 7 shows the experimental and calculated integrated flux for neutron energies greater than 1.0 MeV, for both Ta and ^{238}U irradiations in the direction perpendicular to the target axis (see Fig 1.). The perpendicular dosimetry hole was located ~4 cm from the front face of the target, a position chosen to coincide with the maximum flux along the target axis as calculated prior to these experiments. The calculated position of the flux peak is confirmed in Fig. 8, which shows the experimental and calculated flux distributions (E_n > 1.0 MeV) along the parallel dosimetry direction.

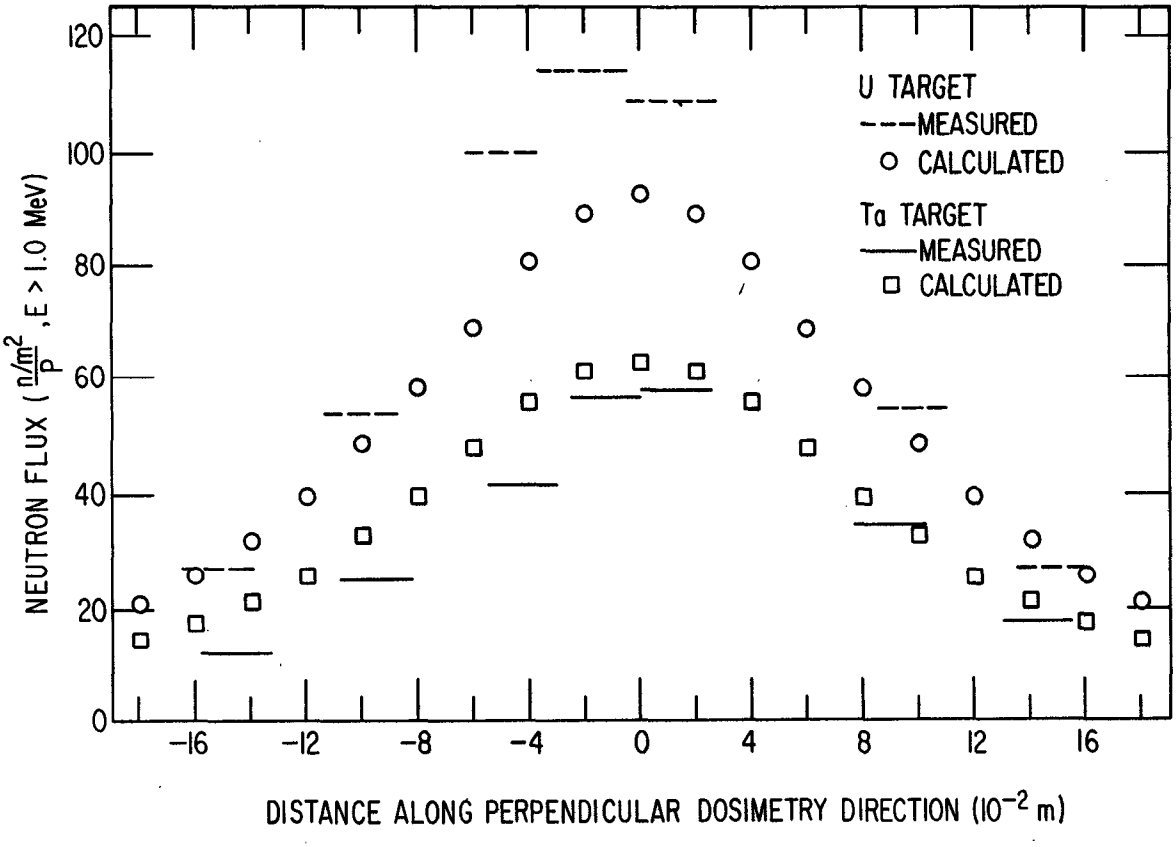

Figure 7. Flux distribution (E_n> 1.0 MeV) along the perpendicular dosimetry direction in the mock-up experiment.

As mentioned above, the fluxes in Figs. 7 and 8 are for neutron energies > 1.0 MeV. The measured peak values of Fig. 7 are the same as those of the principal dosimetry site and have an uncertainty of 11 to 13% (Table 2). The remaining measurements shown in Fig. 7 and all measurements in Fig. 8 were obtained from eight neutron reactions which were fit at each measurement position with the STAYSL computer code, using the neutron spectra obtained at the principal dosimetry site as the input spectra. The resultant neutron spectra and the integrated flux (E_n>1.0 MeV) at each position are uncertain by approximately ±30%. Since the neutron reaction thresholds are above 1 MeV, the uncertainty of integrated flux values for E_n greater than 0.1 MeV in these positions is considerably greater. However, the agreement between measured and calculated fluxes in Fig. 7 and 8 is reasonably good, especially for the Ta target irradiation. The rather larger disagreement in Fig. 8 between experimental and calculated peak flux values for the ^{238}U target must be viewed cautiously, as the uncertainty is larger for these experimental flux values than for the peak values of Fig. 7.

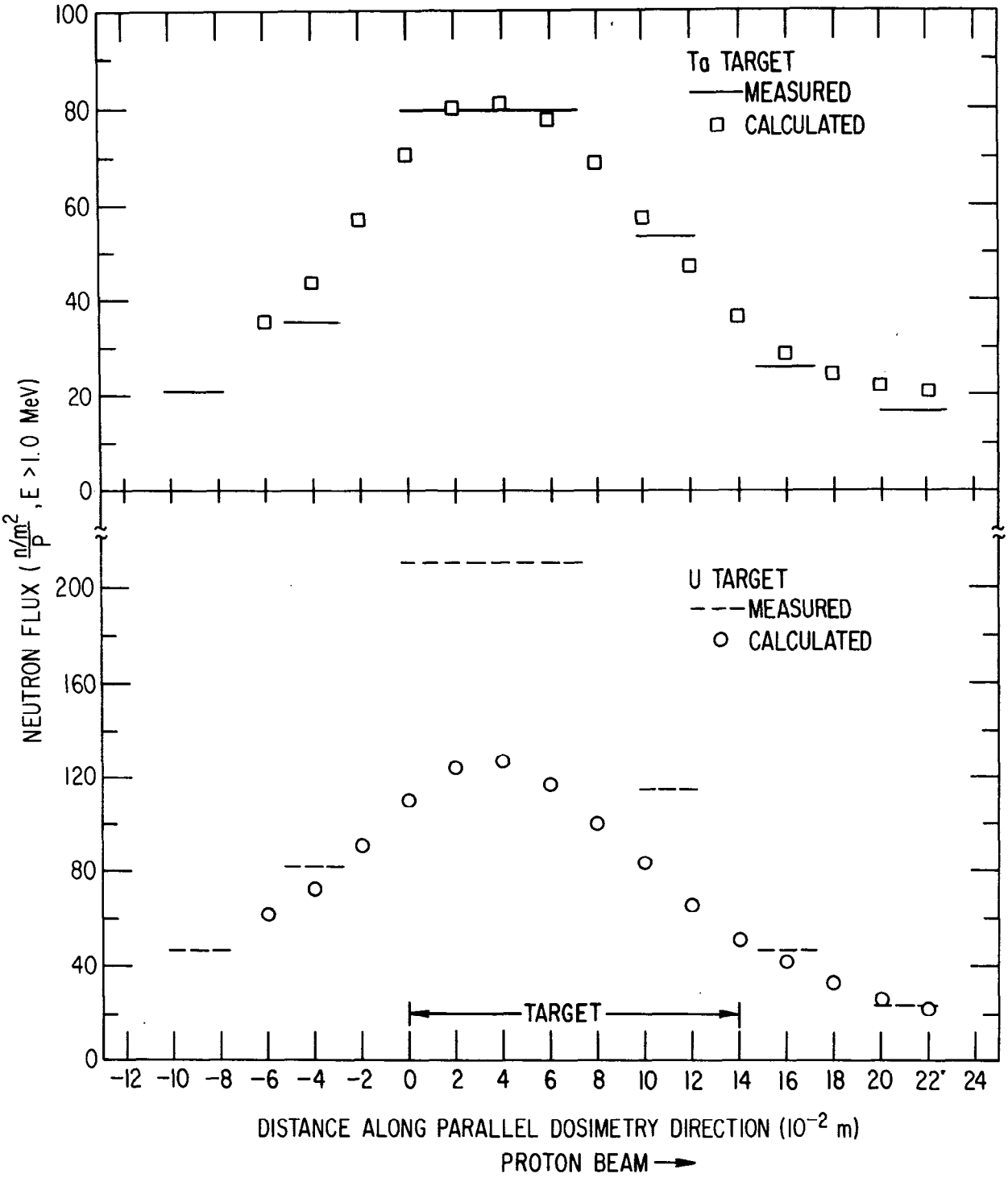

Figure 8. Flux distribution (E_n > 1.0 MeV) along the parallel dosimetry direction in the mock-up experiment.

The accuracy of the spectra above 1.0 MeV is sufficient to make some qualitative statements concerning the variation of these spectra along the two directions. In the perpendicular direction, which is nearly radial, the neutron spectrum above 1.0 MeV softens slightly with increasing distance from either target; the ratio of neutrons above 10 MeV to those above 1.0 MeV is ~30% lower at a location 20 cm out from the primary dosimetry site. In this direction the thermal-neutron flux decreases less sharply than the flux for E_n > 1.0 MeV.

The spectral changes above 1.0 MeV are slight along the direction parallel to the target axis and between the target and reflector. Above 1.0 MeV, the spectrum hardens somewhat with increasing distance behind the front face of the target; the ratio of neutrons above 10 MeV to those above 1.0 MeV is ~20% higher 20 cm from the peak flux position. However, the thermal-neutron flux, measured in front of and behind the target, falls less sharply than the flux for E > 1.0 MeV. This is probably due to the target-cooling systems, since slightly larger volumes of water are located immediately in front of and behind the targets than along their sides.

4.2 REF.

The spatial variation of neutrons with E > 0.1 MeV within the REF thimbles has been determined from the activation of Ni dosimeter wires [^{58}Ni (n,p)^{58}Co]. The fluxes were determined by comparing the measured activities with those measured at the positions of the full spectral dosimetry packages. Any changes in the neutron energy spectrum have been ingnored.

Figure 9 shows the variagion of the neutron flux (E > 0.1 MeV) within the REF vertical thimble. The surfaces of constant neutron flux within the thimble can be approximated by cylinders centered on the ^{238}U target axis. The maximum flux is 311 (n/ m^2)/p at the position nearest the target. The flux decrease within the crystal in a direction perpendicular to the target axis is nearly linear. The 50% decrease across the vertical thimble is larger than the ~30% decrease expected in a solid Pb reflector but the same as the decrease expected in a solid Ta reflector. The difference between these two reflector materials is due to the additional neutron generation in Pb by multiple neutron reactions.

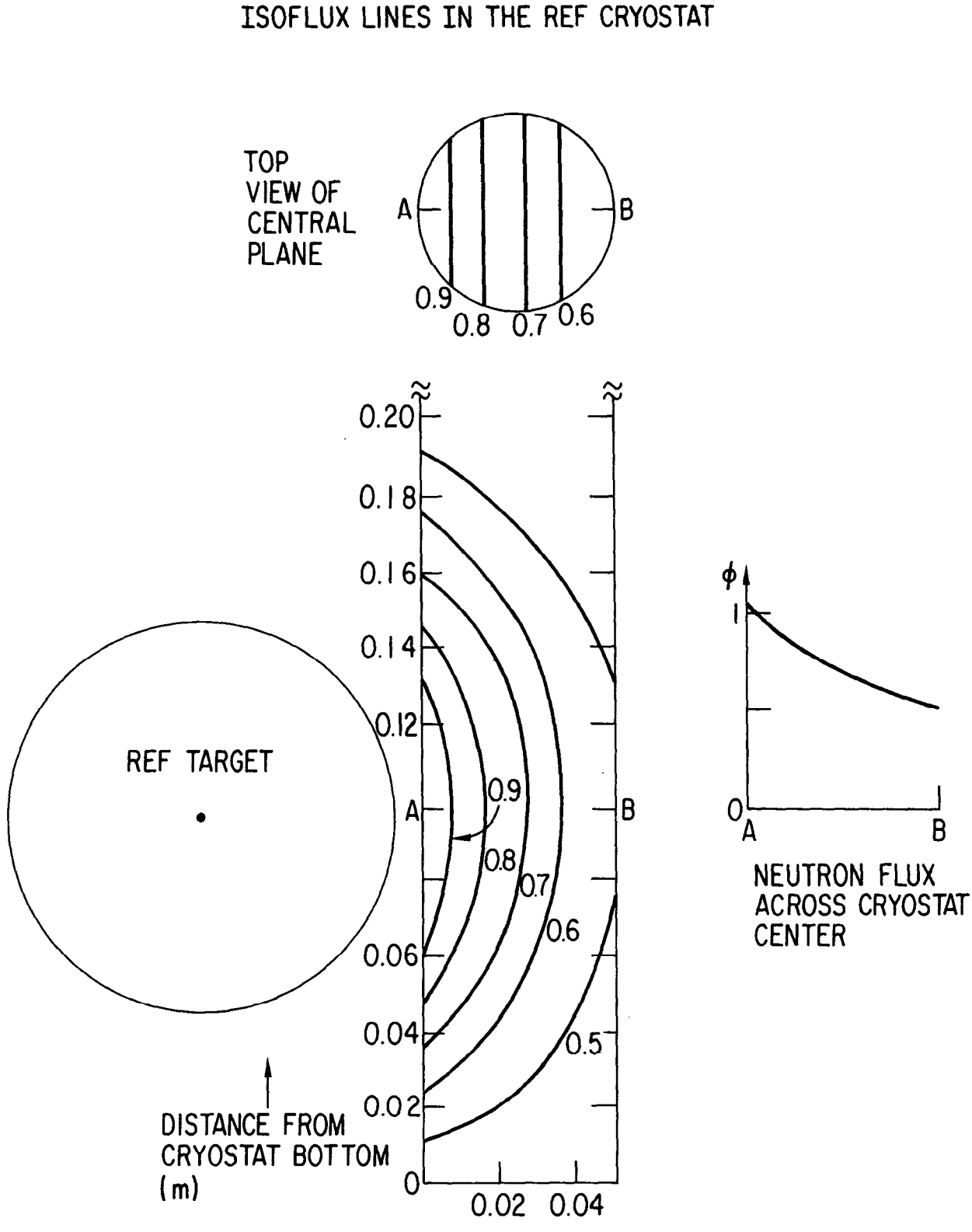

Figure 9. Spatial variation of the neutron flux (E_n > 0.1 MeV) within the REF vertical thimble.

Figure 10 shows the variation of the neutron flux (E > 0.1 MeV) along the length of the REF horizontal thimble located below the ^{238}U target. The neutron flux is a maximum at a position 4-5 cm behind the front face of the ^{238}U target, in agreement with previous calculations. This measurement was made along the bottom of the horizontal thimble. At the top of the horizontal thimble (1.5 cm closer to the target), the flux is 30% higher.

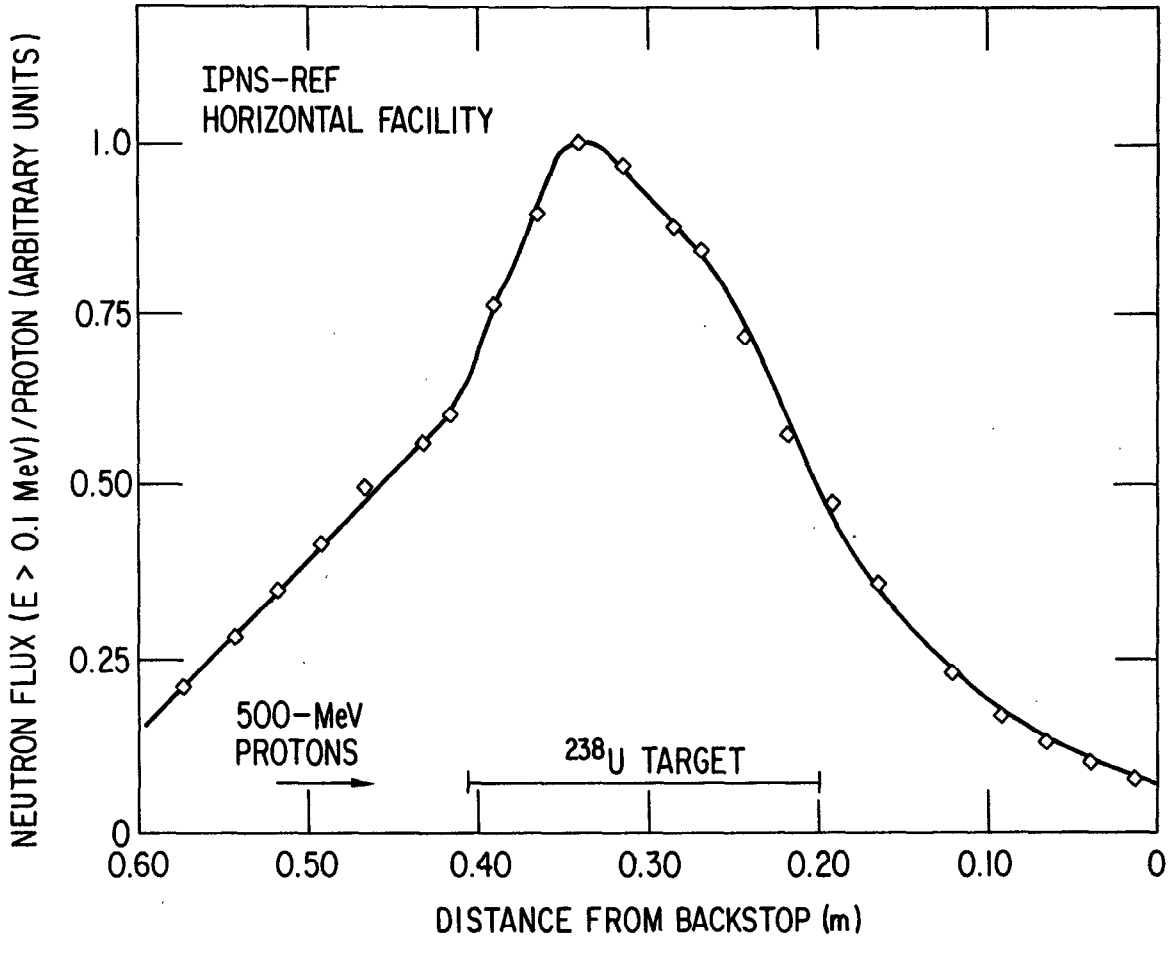

Figure 10. Spatial variation of the neutron flux (E_n > 0.1 MeV) within the REF horizontal thimble.

In the case of the NSF horizontal thimbles, which are nearly radial to the target axis, the neutron flux decreases rapidly with increasing distance from the target. The rate of flux decrease is the same as in the midplane of the REF vertical thimble (Fig. 9).

7. Summary

The neutron spectra, flux and flux spatial distribution for a spallation neturon source have been determined for a simplified system who's geometry allowed computer modeling of the neutron generation. Based on these results, a new neutron source, the IPNS, has recently been constructed at Argonne National Laboratory. This source is a national facility for radiation effects and condensed matter research. The Radiation Effects Facility (REF) has two cryogenic irradiation thimbles and one ambient-temperature irradiation thimble, and the Neutron Scattering Facility has two ambient-temperature irradiation thimbles. The neutron spectra, flux and flux spatial distribution has been determined for each of these thimbles. The large, well-controlled and -instrumented irradiation volume, the well-characterized neutron spectrum and flux, and the dedication to radiation effects studies make the REF ideally suited for both basic and applied research.

Acknowledgments

The authors would like to thank the operators and other personnel associated with the RCS accelerator for their assistance with the irradiations.

References

1.) R. C. Britcher, T. H. Blewitt, M. A. Kirk, T. L. Scott, B. S. Brown and L. R. Greenwood, J. Nucl. Mater. To be published.

2.) M. A. Kirk, R. C. Birtcher, T. H. Blewitt, L. R. Greenwood, R. J. Popek and R. R. Neinrich, J. Nucl. Mater. 96 (1981) 37.

3.) E. A. Crosbie, M. H. Foss, T. K. Khoc and J. D. Simpson, IEEE Trans. Nucl. Sci. NS-22(3) 1975, 1056.

4.) J. Tobailem, C. H. Lassus-St. Genies and L. Leveque, Commissariat a l'Energie Atomique (France) Report No. CEA-N-1446 (1971).

5.) K. C. Chandler and T. W. Armstrong, Oak Ridge National Laboratory Report ORNL-4744 (1972).

6.) E. M. Gelbard and R. E. Prael, Argonne National Laboratory Report ANL-75-2 (1974).

7.) C. W. Potts, IEEE Trans. Nucl. Sci., NS-28 (1981) 2104.

8.) F. G. Perey, Oak Ridge National Laboratory Report ORNL/TM-6062 (1977) as modified by L. R. Greenwood.

9.) R. Malewicki, R. R. Heinrich and R. J. Popek, Proc. 23rd Conf. on Analytical Chemistry in Energy Technology, Radioelement Analysis-Progress and Problems, Gatlinburg, Tnn., Oct. 9-11, (1979) 155.

10.) ENDF/B-IV Dosimetry File, Brookhaven National Laboratory Report BLN-NCS-50446 (1975).

11.) L. R. Greenwood, Argonne National Laboratory Report ANL-FPP/TM-115 (1978).

12.) L. R. Greenwood, R. R. Heinrich, M. J. Saltmarsh and C. B. Fulmer, Nucl. Sci. Eng. 72 (1979) 175.

13.) R. R. Fullwood, J. D. Cramer, R. A. Haarman, R. P. Forrest, Jr., and R. G. Schrandt, Los Alamos Scientific Laboratory Report LA-4789 (1972).